Deuterium Isotope Effects on Reaction Rates of Ground State Zr with Ethylene and Propylene

Meredith Porembski and James C. Weisshaar*

Department of Chemistry, 1101 University Avenue, University of Wisconsin—Madison, Madison, Wisconsin 53706-1396

Received: August 31, 1999; In Final Form: November 30, 1999

Kinetic isotope effects for the reactions of Zr ($4d^25s^2$,^{3}F) with C_2H_4 and C_2D_4 and with C_3H_6 and C_3D_6 are measured in a fast flow reactor at 300 K with He/N_2 buffer gas at 0.8 Torr. The H_2 and D_2 elimination products are detected using single photon ionization at 157 nm and time-of-flight mass spectrometry. We find no significant isotope effect for reaction with either ethylene or propylene. These results clearly favor an indirect mechanism involving addition of the metal atom to the CC double bond and subsequent CH insertion and rule out a recently proposed mechanism involving direct CH bond insertion at low collision energy. Density functional theory in its B3LYP/LANL2DZ form finds no barrier to addition of ground state Zr to the double bond of ethylene and confirms the existence of a low-energy path from the metallacyclopropane complex to H_2 products. Theory also provides a realistic set of geometries and vibrational frequencies for use in a statistical rate model of the hot metallacyclopropane complex decay. However, the RRKM calculations indicate that a small barrier (0.5−2 kcal/mol) to the approach of Zr and ethylene is necessary to explain our kinetics data and the crossed beam angular distributions of Willis et al. In addition, the barrier to CH insertion must be lowered by 3−6 kcal/mol from the B3LYP/LANL2DZ value.

I. Introduction

From a combination of experiment and electronic structure theory, the reactions between gas-phase transition metals and small hydrocarbons provide the opportunity to dissect organometallic reaction mechanisms in unprecedented detail. For the reactions Ni^+ + propane, Ni^+ + *n*-butane, and Co^+ + propane, density functional theory in its B3LYP form found new reaction paths involving rate-determining multicenter transition states (MCTSs) to H_2 or CH_4 elimination products.[1−3] Experimental data combined with statistical rate modeling was then used to adjust the energies of the key MCTSs downward by 5−7 kcal/mol. Angular momentum conservation played a key role by cutting off the reaction probability for large *J*, thus limiting the overall reaction efficiency, although the adjusted MCTSs are located well below the reactant energy.

For reactions of neutral transition metal atoms with alkanes and alkenes, we have measured many reaction rates at 300 K[4−8] and recently learned to identify reaction products using photoionization mass spectrometry (PI/MS) at 157 nm.[9] For example, ground state Zr($4d^25s^2$, ^{3}F) is able to insert in a CH bond of ethylene and eliminate H_2 quite efficiently (20% of the estimated hard spheres collision rate) at room temperature. This sets an upper limit of about 2 kcal/mol on any barrier along the ground state adiabatic reaction path, a challenge to our qualitative notion that repulsive forces between the closed-shell s^2 configuration of the metal and the closed-shell alkene would cause a significant barrier to association.

Theoretical calculations using the scaled configuration interaction theory labeled PCI-80 (Figure 1) are in qualitative agreement with the Zr + C_2H_4 kinetics data.[6] Ethylene was found to bind strongly to an excited state of Zr ($4d^35s^1$,^{3}F),

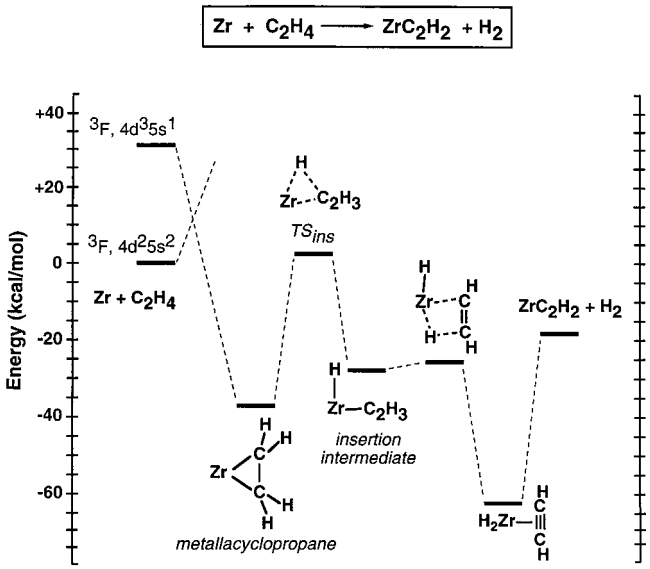

Figure 1. PCI-80 reaction path energetics for Zr + C_2H_4 from ref 6. All energies are measured relative to ground state reactants and corrected for zero-point energy. The crossing of the Zr($4d^25s^2$,^{3}F) and Zr($4d^35s^1$,^{3}F) surfaces may create an entrance channel barrier on the adiabatic path to metallacyclopropane complex formation.

forming a metallacyclopropane complex at −38 kcal/mol relative to ground state reactants. The CH insertion barrier at +1.8 kcal/mol was the largest barrier found on the path to elimination of H_2. However, structural details of TS_{ins} were not reported, and it remains unclear if this saddle point lies on a path connecting the metallacyclopropane complex to the CH insertion intermediate $HZrC_2H_3$. The possible existence of a different rate-determining barrier as *ground state* Zr approaches ethylene was not investigated in detail.

* To whom correspondence should be addressed. E-mail: weisshaar@chem.wisc.edu.

10.1021/jp993082q CCC: $19.00
Published on Web 01/28/2000

Most recently, Willis et al. have reported the first study of the reaction dynamics of Zr + C_2H_4 and Nb + C_2H_4 in a crossed-beam apparatus at collision energies of 5.9, 9.1, and 14.0 kcal/mol.[10] Ground state Zr reacts with C_2H_4 to produce the elimination products ZrC_2H_2 + H_2 at all energies studied. However, at 5.9 kcal/mol there is a marked *absence* of the forward−backward, nonreactive scattering of Zr that would be indicative of the formation of long-lived collision complexes. At the higher collision energies, evidence of long-lived collision complexes emerges; backscattering is relatively weak at 9.1 kcal/mol but significant at 14.0 kcal/mol. Statistical rate modeling with an approximate set of geometries and vibrational frequencies extracted from the PCI-80 calculations suggested two possible mechanisms. First, formation of the metallacyclopropane via the tight barrier TS_{tight} lying at about +2 kcal/mol precedes insertion into a CH bond of ethylene via TS_{ins}, which lies sufficiently far below reactants (−5 kcal/mol) that insertion essentially *always* leads to H_2 elimination at low energy. The onset of backscattered Zr at higher energy is then due to angular momentum constraints at TS_{ins}. Alternatively, a direct CH insertion mechanism could occur but would require a high barrier to addition (roughly 6−9 kcal/mol to match experiment) and a very low barrier to direct insertion (less than about 2 kcal/mol to remain consistent with the reaction efficiency at 300 K).

This paper presents an experimental study of kinetic isotope effects at 300 K for the reactions of Zr with C_2H_4, C_2D_4, C_3H_6, and C_3D_6. The lack of any significant isotope effect rules out the direct CH insertion mechanism at low collision energy and thus indirectly supports the first mechanism involving complex formation prior to CH insertion. To provide essential vibrational frequencies and moments of inertia for RRKM rate calculations, we have performed detailed electronic structure calculations using density functional theory in its B3LYP/LANL2DZ form on the Zr + ethylene system. We search explicitly for a barrier as ground state Zr approaches ethylene to form the complex but find none at this level of theory. We locate the transition state to CH bond insertion (TS_{ins}) and establish that the intrinsic reaction coordinate (IRC, the path of steepest descent) moving away from TS_{ins} leads to the metallacyclopropane complex in one direction and to the insertion intermediate $HZrC_2H_3$ in the other. Finally, we use RRKM statistical rate modeling based on the B3LYP/LANL2DZ results to find the adjusted energies of the key stationary points that bring the model results in accord with all of the experimental data. As indicated before by Willis et al., if the reaction occurs on the adiabatic ground state surface, the data demand a small barrier of 0.5−2 kcal/mol to formation of the metallacyclopropane complex, depending on the location of TS_{tight}. The energy of TS_{ins} must then lie at −4 to −7 kcal/mol, a modest downward adjustment of 3−6 kcal/mol compared with the B3LYP/LANL2DZ result.

II. Experimental Section

An earlier publication describes our flow tube apparatus and the PI/MS technique in detail.[9] Briefly, we use laser ablation to generate gas-phase transition metal atoms in a fast flow of predominately He and some N_2 (added to quench He* and Zr* metastable states). The flow tube temperature is 300 K and the pressure may vary from 0.5 to 1.1 Torr, with N_2 partial pressure constant at 120 mTorr. Frequent collisions with the buffer gas thermalize metal atoms as they travel down the flow tube. In the reaction zone, hydrocarbon flow is regulated by a flow controller and monitored by a mass flow meter (Tylan). Hydrocarbon gases, C_2H_4 (Matheson 99.99%), C_2D_4 (Cambridge Isotopes 98%), C_3H_6 (Matheson 99%), and C_3D_6 (Cambridge Isotopes 98%) were used directly from the bottle. Because flow meter response is not linear with gas flow, we calibrate the flow meters with each reactant gas, measuring pressure vs time while flowing gas into a calibrated volume. Calibration curves for deuterated and undeuterated gases are noticeably different. A skimmer (floated at +8 V) terminates the reaction and permits neutral species to proceed to the detection region where a 157 nm, 7.9 eV laser (Lambda Physik, LPX 210i) ionizes unreacted metal and metal products. The ions are collected via time-of-flight mass spectrometry (TOF-MS).

By measuring integrated ion currents as a function of hydrocarbon flow at a fixed mean reaction time, we extract effective bimolecular rate constants. A variety of complications such as excited-state reactions, ion−molecule reactions, photoionization followed by fragmentation of reaction products, and multiphoton effects have been considered and were found to be minimized under our experimental conditions.[9] Ultimately, the excellent agreement with rate constants derived from state-specific laser-induced fluorescence (LIF) data[5,6] confirms that we are probing ground-state reactions with the PI/MS technique.

III. Experimental Results

Earlier, photoionization results showed that the primary products of the reactions of Zr with C_2H_4 and C_3H_6 are[9]

$$Zr + C_2H_4 \rightarrow ZrC_2H_2 + H_2 \quad (1)$$

$$Zr + C_3H_6 \rightarrow ZrC_3H_4 + H_2 \quad (2)$$

Similarly, we find the primary products of the reactions of Zr with C_2D_4 and C_3D_6 to be

$$Zr + C_2D_4 \rightarrow ZrC_2H_2 + D_2 \quad (3)$$

$$Zr + C_3D_6 \rightarrow ZrC_3H_4 + D_2 \quad (4)$$

A subsequent paper will describe the secondary reactions in detail.[11] Briefly, Zr reacts successively with six molecules of C_2H_4 or C_2D_4 and with four molecules of C_3H_6 or C_3D_6. Alkene addition, rather than elimination of H_2 or D_2, is increasingly favored as the number of ligands surrounding the metal increases.

For all four reactions, the raw PI/MS intensities indicate that collisionally stabilized Zr(alkene) complexes are less than 10% of the primary products over a flow tube pressure range of 0.5 to 1.1 Torr. It remains possible that the photoionization cross section of Zr(alkene) complexes is unusually small and our detection efficiency consequently low. We are, however, able to ionize and readily detect the YC_2D_4, YC_3H_6, and YC_3D_6 products of the analogous reactions of $Y(4d^15s^2, {}^2D)$, as described elsewhere.[11] As argued previously, ionization of stabilized Zr(alkene) complexes followed by H_2 elimination on the $Zr(alkene)^+$ surface is highly unlikely as the source of the observed $Zr(alkyne)^+$ signals.[9]

Representative pseudo-first-order kinetics plots for the Zr + C_2H_4 and Zr + C_2D_4 reactions are shown in Figure 2, emphasizing the quality of the data and the virtually identical rate constants. The resulting effective bimolecular rate constants at 300 K and 0.8 Torr total pressure are collected in Table 1 for all four reactions. Each rate constant is the mean of at least two experiments and in most cases three. The absolute accuracy of our measurements is ±30% due to uncertainties in the mean reaction time, flow calibrations, etc. However, the typical precision of the experiments is much higher. Since most

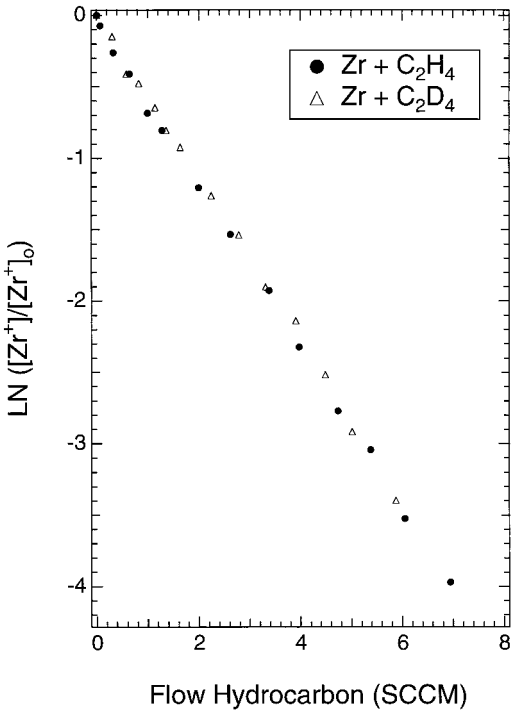

Figure 2. Semilogarithmic plots of metal atom density, proportional to integrated ion current, vs hydrocarbon flow for Zr + C_2H_4 and Zr + C_2D_4 reactions.

TABLE 1: Primary Reaction Products, Effective Bimolecular Rate Constants, and Resulting Isotope Effects for the Reaction of Zr($4d^25s^2$,^{3}F) with Selected Hydrocarbons at 0.8 ± 0.05 Torr of He/N_2 and 300 ± 5 K

hydrocarbon reactant	primary reaction product[a]	k (10^{-12} cm^3 s^{-1})[b]	k_H/k_D
C_2H_4	ZrC_2H_2	55 ± 1	
C_2D_4	ZrC_2D_2	53 ± 1	1.04 ± 0.04
C_3H_6	ZrC_3H_4	135 ± 6	
C_3D_6	ZrC_3D_4	130 ± 6	1.04 ± 0.09

[a] Inferred from photoionization mass spectra. [b] Uncertainties refer to the precision of experiments. Absolute accuracy of rates is ±30%.

systematic errors should cancel for ratios of rate constants and we have corrected for different flow calibrations, we estimate that the ratios k_H/k_D in Table 1 are accurate to within ±5% for the reaction with ethylene and ±10% for the reaction with propylene. Within experimental uncertainty, there is no deuterium isotope effect with either ethylene or propylene.

IV. Theoretical Results

A. Ab Initio Calculations. Blomberg and Siegbahn have already used electronic structure theory to study the Zr + C_2H_4 reaction.[6,12−14] In the most recent study, stationary point geometries were optimized at the Hartree−Fock level and relative energies (corrected for zero-point energies) were computed using modified coupled pair functional (MCPF) theory corrected by the PCI-80 approximation (Figure 1).[6] Geometry optimizations used double-ζ quality basis sets, while larger sets including polarization functions on Zr were used for energy calculations.

Here, we use B3LYP density functional theory with the modest LANL2DZ basis set of the Gaussian 98 program to augment the earlier studies.[15] First, we search for a possible barrier to addition of ground state Zr($4d^25s^2$, ^{3}F) to the alkene double bond. When the approach of the metal atom is constrained to lie on the perpendicular bisector of the CC bond

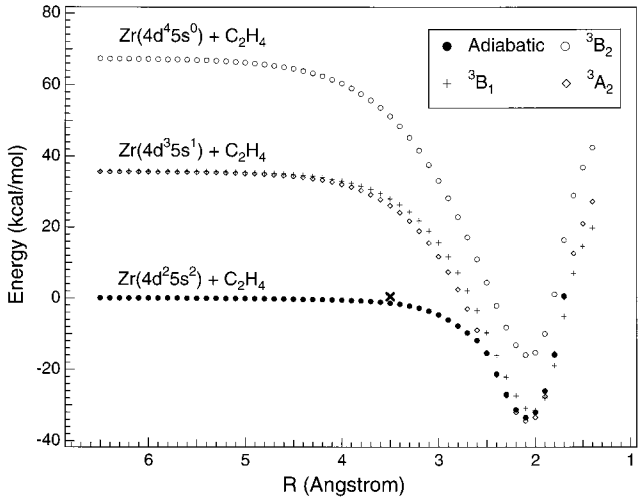

Figure 3. B3LYP/LANL2DZ energies (uncorrected for zero-point energy) along the reaction path Zr + C_2H_4 → ZrC_2H_4 for a number of triplet molecular symmetries. R is the approach distance between Zr and ethylene as described in the text. The single point at R = 3.5 Å marked by X was optimized at the B3LYP/Stuttgart+6-311++G(d,p) level of theory; see text.

and the overall geometry is constrained to C_{2v} symmetry, the calculations preserve the initial electronic symmetry and (roughly) the 4d orbital occupancies as the approach distance R scans toward larger values. Figure 3 presents three of the resulting triplet diabatic electronic states ($^3B_1$, $^3B_2$, and $^3A_2$), each of which smoothly dissociates to a particular electronic state of Zr. The three curves differ in metal atom orbital occupancy; they are quite similar in energy in the region of chemical bonding and in equilibrium bond length. The computed atomic excitation energy from the Zr($4d^25s^2$, ^{3}F) ground state to the excited state Zr($4d^35s^1$, ^{3}F) at this level of theory is 36 kcal/mol, in good agreement with the experimental excitation energy of 32 kcal/mol.[16] The latter state is important in forming covalent chemical bonds, and the agreement between experiment and theory suggests that energies of chemically bound species relative to reactants will be realistic. The triplet $4d^4$ state to which the $^3B_2$ molecule dissociates is unknown experimentally.

The geometry of the $^3A_2$ state of the metallacyclopropane complex (the global minimum) and its energetics are described in Figure 4A and Table 2. We call the complex a metallacyclopropane species based on its short ZrC bonds and long CC bond; the π bond is essentially broken at the potential minimum. The PCI-80 calculations described above found the $^3B_1$ state to be the minimum, whereas B3LYP/LANL2DZ finds it to be an excited state lying only 2 kcal/mol above the ground state complex. The geometries and energetics are very similar for the two different states and for the two different theoretical treatments.

When the C_{2v} symmetry constraint is relaxed by tilting the approach axis by 5° simultaneously in both symmetry planes while continuing to "aim" the metal atom towards the midpoint of the CC bond, the molecule loses all symmetry elements. In this way, we compute the adiabatic ground state potential energy curve shown in Figure 3. At the B3LYP/LANL2DZ level of theory, we find no barrier to the approach of Zr and ethylene. At R = 3.5 Å, the bare potential lies at −1.5 kcal/mol relative to reactants. The standard counterpoise estimate of the basis set superposition error (BSSE) is +0.6 kcal/mol, so there would be no barrier with LANL2DZ even if we applied this correction.

Next, we locate the CH insertion intermediate $HZrC_2H_3$. Its geometry and energetics are described in Figure 4C and Table

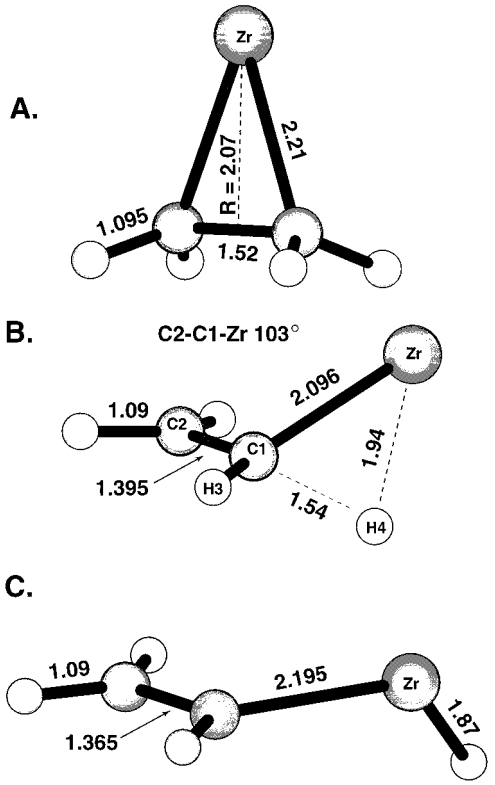

Figure 4. B3LYP optimized geometries for the metallacyclopropane complex (A), TS_{ins} (B), and the insertion intermediate $HZrC_2H_3$ (C). Distances are in angstroms.

TABLE 2: Calculated Energies (kcal/mol) of Potential Minima and Saddle Points for the Reaction of Zr with Ethylene[a]

species	bare potential[b] B3LYP	$Zr + C_2H_4$[c] B3LYP	$Zr + C_2H_4$[c] PCI-80	$Zr + C_2D_4$[c] B3LYP
$Zr(C_2H_4)$	−34.5	−35.1	−38.0	−35.0
TS_{ins}	+3.0	−1.4	+1.8	−0.2
$HZrC_2H_3$	−26.2	−30.2	−28.7	−29.2

[a] B3LYP entries refer to this work; PCI-80 calculations by Blomberg and Siegbahn from ref 6. [b] Energies relative to free reactants, uncorrected for zero-point energy. [c] Energies relative to free reactants, corrected for differential zero-point energy effects.

2. The CC double bond is essentially restored in this ethylenic intermediate for which the two carbons, Zr, and three hydrogens lie approximately in a plane.

Finally, we locate the transition state TS_{ins} that has been assumed to connect the complex to the CH insertion intermediate $HZrC_2H_3$. Its geometry and energetics are described in Figure 4B and Table 2. The transition state is not planar; Zr lies above and H_4 lies below the plane formed by $C_2C_1H_3$. To confirm the earlier assumption that TS_{ins} is the saddle point between the metallacyclopropane complex and the CH insertion intermediate, we followed the IRC leading away from TS_{ins} in both directions. The geometries at the terminal points of these scans are illustrated in Figure 5. In particular, it is clear that in moving toward the left the geometry is approaching that of the metallacyclopropane complex, with Zr−C distances shortening and all four hydrogens bending out of the plane of ethylene. Toward the right, the geometry approaches the nearly planar configuration of the insertion intermediate as the angles C_2-C_1-Zr and C_1-Zr-H_4 increase to roughly 120°.

We find no evidence of dissociation from TS_{ins} toward $Zr + C_2H_4$. It had been suggested earlier that perhaps the insertion transition state *first* reported by Blomberg and Siegbahn lay between *reactants* and the CH insertion intermediate, as would occur for a direct insertion mechanism.[13] That species does differ slightly from TS_{ins} depicted in Figure 4B; the former geometry is defined by $Zr-C_1$ and $Zr-H_4$ distances of 2.25 and 2.12 Å, respectively, and an angle C_2-C_1-Zr of 126.2°. The geometry of the insertion transition state of ref 6 (Figure 1 and Table 2) has not been reported, although its energy compares favorably with the B3LYP/LANL2DZ calculations of this work. To explore the possibility of low-energy routes to direct CH insertion, we searched for a variety of paths on which Zr approached the $-CH_2$ end of ethylene rather than the double bond. The potential energy always rose steeply on approach paths for which the metal atom was remote from the double bond, whose participation seems essential to the low-energy activation of the CH bond.

TABLE 3: B3LYP Vibrational Frequencies (cm^{-1}) and Rotational Constants (cm^{-1}) Used in RRKM Calculations for $Zr + C_2H_4$ Reaction

TS_{orb}[a]	TS_{tight}[b]	metallacyclopropane	TS_{ins}
3276	3276	3166	3217
3238	3240	3142	3146
3169	3169	3078	3119
3143	3144	3061	1524
1678	1670	1452	1500
1487	1488	1436	1305
1388	1385	1195	1211
1246	1247	1032	988
1055	1057	967	887
1011	1012	881	823
999	1008	779	616
843	843	544	597
	120	475	436
	70	466	102
		460	
4.888	0.823	0.716	1.022
0.983	0.049	0.168	0.132
0.818	0.047	0.144	0.120

[a] Values are those calculated for C_2H_4, appropriate for a loose model of the transition state to dissociation (TS_{orb}). [b] We alternatively model the transition state to dissociation as tight (TS_{tight}); see text for details. Values are those calculated from a geometry optimization of the complex with R fixed at 4.0 Å (Figure 4A).

For stationary points corresponding to the entrance channel transition state (either TS_{orb} or TS_{tight} defined below), the metallacyclopropane complex and TS_{ins}, we computed harmonic vibrational frequencies for use in the rate modeling below. The frequencies and rotational constants are collected in Table 3.

To test basis set effects, we repeated a few of the calculations using the Stuttgart ECP + valence set for Zr[17] and a much larger basis for C and H as well. We call this B3LYP/Stuttgart+6-311++G(d,p). For both $Zr + C_2H_4$ and TS_{ins}, we optimized both geometries and corrected for zero-point energy. The energy of TS_{ins} relative to reactants *increased* by 3.4 kcal/mol to +2.0 kcal/mol compared with the B3LYP/LANL2DZ result of −1.4 kcal/mol. This result is very close to the earlier value of 1.8 kcal/mol from Blomberg and Siegbahn[6] using the PCI-80 adjustment. The new frequency set and moments of inertia remain essentially the same. We also calculated the energy of $Zr + C_2H_4$ at the approach distance $R = 3.5$ Å (Figure 3), reoptimizing all other degrees of freedom. Intriguingly, the bare potential energy becomes +0.5 kcal/mol relative to $Zr + C_2H_4$, very close to the small barrier demanded by the RRKM calculations described below. The counterpoise estimate of BSSE is only +0.04 kcal/mol with the Stuttgart+6-311++G(d,p) basis set. The corresponding B3LYP/LANL2DZ result at $R = 3.5$ Å was −1.5 kcal/mol (−0.9 kcal/mol including counterpoise correction for BSSE).

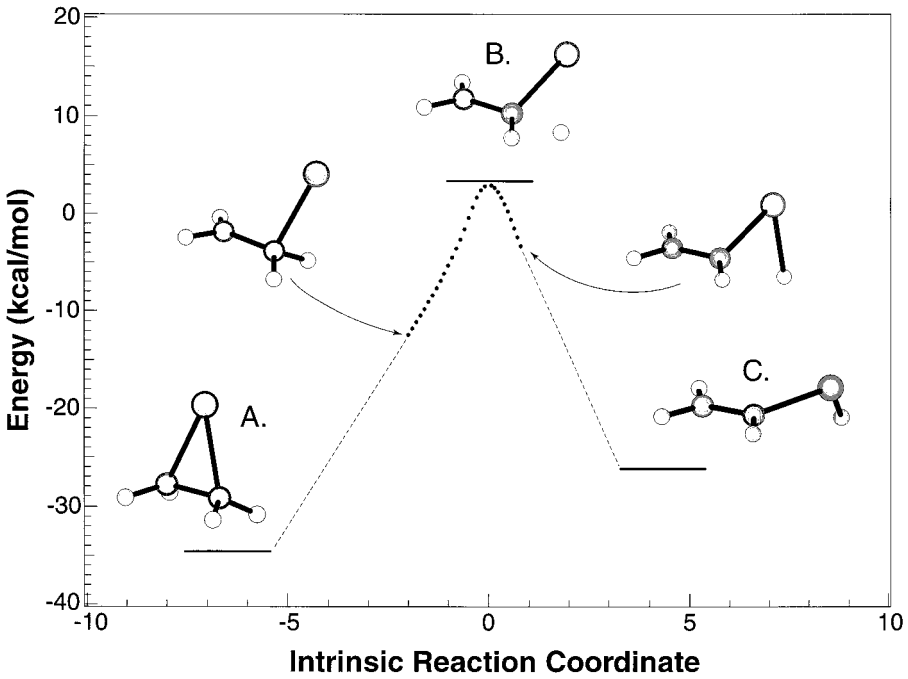

Figure 5. B3LYP energies (●) along the IRC that leads from TS_{ins} (B) to the complex (A) in one direction and the insertion intermediate (C) in the other. Energies, relative to free reactants, are *not* corrected for zero-point energy.

B. Statistical Rate Model. To further elucidate the mechanism of Zr + ethylene, we use the electronic structure results to build a statistical model of the decay of the long-lived metallacyclopropane complex (RRKM theory[18−20]) to explain all available data. Geometries and harmonic frequencies from the B3LYP calculations should permit more realistic modeling than in a previous effort. The energies of key transition states will be adjusted to fit experiment. In the model, long-lived ZrC_2H_4 complexes are formed at a rate k_f and decay into two parallel channels, dissociation back to reactants (k_{diss}) and insertion into a CH bond (k_{ins}). We assume that all insertion intermediates $HZrC_2H_3$ go on to eliminate molecular H_2.

The bulk kinetics data at 300 K and 0.5−0.8 Torr buffer gas include the bimolecular rate constant for $Zr + C_2H_4$, $k = 55 \times 10^{-12}$ cm^3 s^{-1}; the absence of a kinetic isotope effect, $k_H/k_D = 1.04 \pm 0.05$; and the absence of collision complexes sufficiently long lived to be stabilized by a third-body collision, setting an upper bound of approximately 300 ns on the complex lifetime. The crossed-beam data at 5.9 and 9.1 kcal/mol collision energy require formation of H_2 elimination products at both energies, with the onset of backscattering of nonreactive Zr at the higher energy. Specifically, $k^H_{diss}/k^H_{ins} \approx 0.05$ at 5.9 kcal/mol, as estimated from the experimental detection sensitivity; the ratio should be slightly larger at 9.1 kcal/mol, the collision energy at which backscattered Zr is first weakly observed.[10]

Our model calculations are somewhat oversimplified; they are intended to demonstrate that a range of plausible model energetic parameters can explain all of the data. The connection between the model and the experimental data is made via the microcanonical rate constant:

$$k(\bar{E}) = \sum_{J=0}^{J_{max}} P(J)\, k(\bar{E},J)$$

$$= \sum_{J=0}^{J_{max}} P(J)\, k_f(\bar{E}_t) \frac{k_{ins}(\bar{E},J)}{k_{ins}(\bar{E},J) + k_{diss}(\bar{E},J)} \qquad (5)$$

Here $\bar{E}$ is the mean total energy, $\bar{E}_t$ is the mean collision (translational) energy, and J is the total angular momentum of the complex. The J distribution is $P(J) = 2J/J_{max}^2$, where J_{max} is the largest value of J for the metallacyclopropane complexes. For the sake of simple comparisons with the bulk kinetics data, we carry out microcanonical rate calculations at a collision energy which we call $\bar{E}_t$, the average energy of those thermal collisions that can surmount the assumed entrance channel barrier for zero-impact parameter collisions. The barrier E_{barr} itself is adjusted to lie in the range 0−2 kcal/mol; correspondingly, the treatment of the entrance channel transition state varies from *loose* (TS_{orb}) to *tight* (TS_{tight}). The mean total energy of the complex $\bar{E}$ includes $\bar{E}_t$ and also the mean vibrational energy of ethylene at 300 K, which is 0.12 kcal/mol, but no rotational energy of reactants. The total angular momentum of the complex is $\vec{J} = \vec{l} + \vec{j}$, where $\vec{l}$ is the orbital angular momentum of the collision and $\vec{j}$ is the rotational angular momentum of the ethylene collision partner. In practice, we assume $\vec{j} = 0$ so that $\vec{J} = \vec{l}$ and there is no rotational energy contributed to the reaction rate. The distribution of total angular momentum in the complex is then the same as the distribution of orbital angular momenta described below.

Each unimolecular rate constant in eq 5 is computed from the usual RRKM expression by a program based on the work of Yi et al.[1] In the rovibrational sum and density of states, we approximate each geometry as a prolate symmetric top and rotation about K is treated as active, while J is conserved. For k_{ins}, the transition state TS_{ins} is modeled as *tight* with the parameters given in Table 3. For k_{diss} in the case $E_{barr} = 0$, as found by B3LYP/LANL2DZ theory, the transition state TS_{orb} is *loose* with the parameters included in Table 3. The 12 vibrations are those of free ethylene and the two soft bends of the complex have been replaced by the two-dimensional free internal rotation of ethylene. The placement of TS_{orb} is determined as the maximum of the effective potential for Zr + C_2H_4 collisions characterized by ($\bar{E}_t$,J) in a kind of variational transition state theory:

$$V_{\text{eff}}(R,J) = -\frac{C_6}{R^6} + \frac{\hbar^2 J(J+1)}{2\mu R^2} \qquad (6)$$

where R is defined as the distance from Zr to the center of mass of C_2H_4, μ is the reduced mass of the collision pair, and $C_6 = 11.3 \times 10^3$ Å^6 kcal/mol.[21] For fixed $\bar{E}_t$, the value of C_6 sets an upper limit on the range of orbital angular momentum that can penetrate the peak in V_{eff}; J varies from 0 to $l_{\max}$ and is weighted as $P(J) = 2J/l^2_{\max}$. For $\bar{E}_t = 0.9$ kcal/mol, $l_{\max} = 122$ and the position of the centrifugal barrier lies at $R_{\max} \approx 6$ Å. For comparison to absolute 300 K rate constants, we compute the rate of association, $k_f = \pi b_{\max}{}^2 \bar{v} = \pi l_{\max}{}^2/\mu^2 \bar{v}$, where $\bar{v}$ is the relative velocity at $\bar{E}_t$. For $\bar{E}_t = 0.9$ kcal/mol, $k_f = 7.5 \times 10^{-10}$ cm^3 s^{-1}; according to this model, the Zr + C_2H_4 reaction is only 7% efficient at room temperature.

The results of the RRKM calculations assuming the loose, orbiting transition state TS_{orb} along the approach path are collected in Table 4 for a variety of assumptions about the energy of TS_{ins}. Superscripts H or D on rate constants refer to the reaction Zr + C_2H_4 or Zr + C_2D_4, respectively. Vibrational frequencies, rotational constants, and other input parameters are suitably modified for calculations of Zr + C_2D_4. Taken together, the absence of an isotope effect at 300 K and the absence of backscattered Zr at 5.9 kcal/mol require that k_{ins} *dominate* k_{diss} at both collision energies. When the insertion barrier is taken at −1.4 kcal/mol relative to reactants ($\Delta E_{ins} = 0$) as obtained by B3LYP, the overall rate constants k_H and k_D are too small and the isotope effect k_H/k_D is far too large at $\bar{E}_t = 0.9$ kcal/mol. In this case, complexes dissociate much faster than they insert. As TS_{ins} is lowered, the rate of insertion increases; the effects are shown in the table. The ratio k_H/k_D decreases to 1.06 when $\Delta E_{ins} = -10$ kcal/mol; at the same time, the ratio k^H_{diss}/k^H_{ins} at $\bar{E}_t = 5.9$ kcal/mol diminishes only to 1.1, in which case backscattered Zr would still be detected in the crossed-beam experiment. Only for $\Delta E_{ins} = -15$ to −20 kcal/mol is the backscattered Zr shut off within the estimated sensitivity of the experiment (see footnote c in Table 4). While it is imaginable that theory is very badly wrong, in the same limit of very low TS_{ins} there is the additional problem that the overall 300 K reaction rates become too large. We discuss the possible effects of a "steric factor" or of nonadiabatic effects on reaction efficiency below.

The alternative assumption models the transition state to association/dissociation as *tight,* with rate-limiting transition state TS_{tight} of energy E_{barr}. Since the calculations found no such barrier to association, the placement of TS_{tight} is somewhat arbitrary; we experiment with $R_{tight} = 2.8$ and 4.0 Å. Vibrational frequencies and rotational constants for TS_{tight} are computed from an optimization of the complex geometry with R_{tight} fixed to the appropriate distance. Table 3 includes the results for the calculations with $R_{tight} = 4.0$ Å. We find that interpolation between the vibrations of the complex and free ethylene leads to a slightly different frequency set, but virtually the same conclusions of the statistical rate model.

To account approximately for the effects of a real potential energy barrier on reaction efficiency, first we calculate f_{thresh}, the fraction of the 300 K Boltzmann distribution with kinetic energy above the threshold for $l = 0$, including differential zero-point energy effects. For each barrier height E_{barr}, we then carry out microcanonical RRKM rate calculations for which $\bar{E}_t$ is now defined as the *mean kinetic energy of that fraction of collisions with energy above threshold.* Inclusion of TS_{tight} at either distance further constrains the range of J that is able to reach the metallacyclopropane complex. We define $J'_{\max} = l'_{\max}$ as the maximum orbital angular momentum that can surmount the centrifugal barrier to reach the complex for a given E_{barr}, kinetic energy $\bar{E}_t$, and corresponding value of R_{tight}. With these definitions, the association rate becomes $k_f = f_{thresh}(\pi b'_{\max}{}^2)\bar{\nu}'$, where $\bar{\nu}'$ is the relative velocity corresponding to $\bar{E}_t$ and $J'_{\max} = \mu\bar{\nu}' b'_{\max}$. For example, for $E_{barr} = 1$ kcal/mol and $R_{tight} = 4.0$ Å, we find $\bar{E}_t = 1.7$ kcal/mol and $J'_{\max} = 71$. The corresponding association rate constant is only $k_f = 6.1 \times 10^{-11}$ cm^3 s^{-1}, a factor of 12 smaller than the association rate constant in the absence of an approach barrier, significantly altering the view of room-temperature reaction efficiency.

Using the TS_{tight} model, RRKM calculations were performed for two values of R_{tight}, 2.8 and 4.0 Å, at various values of E_{barr} (not greater than 2 kcal/mol) and ΔE_{ins}. The resulting RRKM rates for a particular combination of R_{tight} (4.0 Å) and E_{barr} (1 kcal/mol) that fit the experimental data comfortably are shown in Table 5. Comparing Tables 4 and 5, the primary effect of the TS_{tight} model is to decrease k_f and k_{diss} drastically at a given collision energy. Dissociation (k_{diss}) slows because the free rotations of ethylene no longer contribute as active degrees of freedom to the sum and density of states of TS_{tight}. Consequently, TS_{ins} only need be lowered by 4 kcal/mol compared with the B3LYP result in order to explain the absence of both the isotope effect and the backscattering of Zr at 5.9 kcal/mol. The small

TABLE 4: RRKM Rate Constants Assuming Loose TS_{orb}[a]

		ΔE_{ins} (kcal/mol)[b]		
$\bar{E}_t$ (kcal/mol)	rate or ratio	0	−5	−10
0.9	$k^H_{ins}(10^8$ s$^{-1})$	0.06	4.16	135
	$k^D_{ins}(10^8$ s$^{-1})$	0.0016	0.39	24.8
	k_H (10^{-12} cm^3 s^{-1})	25.8	443	746
	k_D (10^{-12} cm^3 s^{-1})	3.39	265	702
	k_H/k_D	7.61	1.67	1.06
5.9[c]	k^H_{diss}/k^H_{ins}		3.1	1.1

[a] At $\bar{E}_t = 0.9$ kcal/mol, the estimated association rates for Zr + C_2H_4 and Zr + C_2D_4 are $k^H_f = 7.5 \times 10^{-10}$ cm^3 s^{-1} and $k^D_f = 7.1 \times 10^{-10}$ cm^3 s^{-1}. The computed complex dissociation rates are $k^H_{diss} = 1.8 \times 10^8$ s^{-1} and $k^D_{diss} = 4.4 \times 10^7$ s^{-1}. At $\bar{E}_t = 5.9$ kcal/mol, $k^H_{diss} = 1.9 \times 10^{10}$ s^{-1}. [b] Amount by which TS_{ins} is lowered for each column of RRKM calculations compared with the B3LYP/LANL2DZ result, which places TS_{ins} at −1.4 kcal/mol relative to Zr + C_2H_4 reactants. Zero-point effects are included. [c] At $\bar{E}_t = 5.9$ kcal/mol, for $\Delta E_{ins} = -15$ kcal/mol, $k^H_{diss}/k^H_{ins} = 0.10$; for $\Delta E_{ins} = -20$ kcal/mol, $k^H_{diss}/k^H_{ins} = 0.012$.

TABLE 5: RRKM Rate Constants Assuming Tight TS_{tight} ($R_{tight} = 4.0$ Å)[a]

		ΔE_{ins} (kcal/mol)[b]		
$\bar{E}_t$ (kcal/mol)	rate or ratio	0	−2	−4
1.7	k^H_{ins} (10^8 s^{-1})	0.37	2.60	12.5
	k^D_{ins} (10^8 s^{-1})	0.016	0.207	1.46
	k_H (10^{-12} cm^3 s^{-1})	58.7	61.5	61.9
	k_D (10^{-12} cm^3 s^{-1})	42.1	57.8	59.1
	k_H/k_D	1.39	1.07	1.05
5.9	k^H_{diss}/k^H_{ins}	0.95	0.22	0.06
9.1[c]	k^H_{diss}/k^H_{ins}	2.35	0.70	0.23

[a] At $\bar{E}_t = 1.7$ kcal/mol, the estimated association rates for Zr + C_2H_4 and Zr + C_2D_4 are $k^H_f = 6.1 \times 10^{-10}$ cm^3 s^{-1} and $k^D_f = 5.9 \times 10^{-10}$ cm^3 s^{-1}. The computed complex dissociation rates are $k^H_{diss} = 2.2 \times 10^6$ s^{-1} and $k^D_{diss} = 5.6 \times 10^5$ s^{-1}. At $\bar{E}_t = 5.9$ kcal/mol, $k^H_{diss} = 1.1 \times 10^8$ s^{-1} and at 9.1 kcal/mol, $k^H_{diss} = 7.7 \times 10^8$ s^{-1}. [b] Amount by which TS_{ins} is lowered for each column of RRKM calculations compared with the B3LYP/LANL2DZ result, which places TS_{ins} at −1.4 kcal/mol relative to Zr + C_2H_4 reactants. Zero-point effects are included. [c] At $\bar{E}_t = 9.1$ kcal/mol and $\Delta E_{ins} = -6$ kcal/mol, $k^H_{diss}/k^H_{ins} = 0.08$ and backscattered Zr would just be detected within experimental sensitivity.

entrance barrier limits the 300 K reaction efficiency and angular momentum effects backscatter Zr at 9.1 kcal/mol. Willis et al.[10] reached similar conclusions without the benefit of the B3LYP results.

Further RRKM calculations reveal how the collection of experimental data constrains the range of acceptable parameters. Values of E_{barr} greater than 1 kcal/mol rapidly decrease reaction efficiency. TS_{ins} may not be lowered too much or Zr is not backscattered at 9.1 kcal/mol (see footnote c in Table 5). In the "tighter" model of TS_{tight} ($R_{tight} = 2.8$ Å), k_f and k_{diss} are further decreased with the result that even smaller values of E_{barr} (0.5 kcal/mol) and higher energy of TS_{ins} (−4 kcal/mol) give rates that remain consistent with experimental data. However, backscattering of Zr at higher collision energies requires that the centrifugal barrier grow faster over TS_{ins} than TS_{tight}, and consequently R_{tight} must not be too small.

Finally, we must consider the absence of stabilized collision complexes. In the flow tube at 0.8 Torr total pressure, quenching occurs via collisions with the buffer gas (mostly He) at a rate $k_Q[He] \approx 3 \times 10^6$ s^{-1}. This estimate uses $k_Q = 1 \times 10^{-10}$ cm^3 s^{-1}, some 5 times smaller than the hard-spheres collision rate because lack of vibrational or rotational degrees of freedom make He a rather inefficient quencher. According to the PI/MS data, for both Zr + C_2H_4 and Zr + C_2D_4, stabilized complexes contribute no more than 10% to the primary products as described above. The RRKM calculations (Table 5) find that the preferred parameters of $E_{barr} = 1$ kcal/mol, $\bar{E}_t = 1.7$ kcal/mol, and $\Delta E_{ins} = -4$ kcal/mol predict $k_{diss} + k_{ins} \approx 10^9$ s^{-1}. Thus, $k_Q[He] \ll k_{diss} + k_{ins}$, consistent with experimental data.

V. Discussion

Our work effectively rules out several mechanistic possibilities raised by the recent crossed-beam measurements.[10] Most importantly, the absence of a measurable deuterium isotope effect in the 300 K rate constant rules out direct insertion of Zr into a CH bond as the first step in the reaction of Zr with either ethylene or propylene. Direct insertion would lead to a large primary isotope effect, as indicated by the RRKM modeling of Zr + ethylene. The same sum of states that appears in the calculation of k_{ins} would appear in a transition state theory expression for the direct insertion rate. Using the parameters for TS_{ins} ($R_{tight} = 4.0$ Å) at $\bar{E}_t = 1.7$ kcal/mol, our model (Table 5) suggests a primary isotope effect k_{ins}^H/k_{ins}^D that decreases from 23 for $\Delta E_{ins} = 0$ to 9 for $\Delta E_{ins} = -4$ kcal/mol, i.e., the primary isotope effect will be large for all reasonable barriers to direct insertion. In the stepwise association/insertion mechanism, this primary isotope effect is concealed in the overall rate k_H because insertion is not rate determining, i.e., $k_{ins} \gg k_{diss}$. Moreover, at least at the B3LYP/LANL2DZ level of theory, the low-lying barrier to CH insertion has now been shown to connect the metallacyclopropane well to the CH insertion well, and no low-energy paths to direct insertion were found. The evidence that attack of the CC double bond precedes CH insertion for Zr + C_2H_4 is by now overwhelming.

The remaining issues involve the height of the barrier to CH insertion and the possible presence of a small barrier to association. In the absence of an experimentally measured threshold energy for H_2 elimination, we must try to address these related questions based on the RRKM modeling. If there is no barrier to association, then the absence of an isotope effect at 300 K and the onset of backscattered Zr above 9.1 kcal/mol seemingly demand that TS_{ins} lie far below the value of −1.4 kcal/mol found by B3LYP. In fact, a value of −16 kcal/mol is just comfortable. Even if theory were so badly wrong, we would still need to explain the inefficiency of a reaction that has no barrier to association and only a very low subsequent barrier to CH insertion. One possibility is a steric effect; perhaps many approach angles are repulsive and many collisions fail to "find" the cone of attractive approach angles. An effective counter argument is that the reactions Zr + C_3H_6 and Nb + C_2H_4 are 2.5 and 6 times *more* efficient,[11] respectively, than Zr + ethylene, suggesting that internal rotation within the complexes allows the metal atom to find the attractive cone.

Another possible origin of reaction inefficiency is nonadiabatic effects. The predominant $J = 2$ level of the $Zr(4d^25s^2,{}^3F)$ ground state is 5-fold electronically degenerate. Some of the resulting triplet potentials are likely repulsive, since they aim valence metal d orbitals in the wrong directions in space for effective bonding to the alkene. Perhaps the Zr + C_2H_4 reaction is inefficient at 300 K because a substantial fraction of collisions remains on these repulsive potentials long enough to approach and recede without making a nonradiative transition onto the strongly attractive adiabatic potentials. It remains necessary to assert that all collisions that reach the strongly attractive potentials go on to eliminate H_2 so that no backscattering of Zr occurs at low energy. If the reaction efficiency is determined primarily by these long-range electronic factors, the deuterium isotope effect could be small or even inverse ($k_H < k_D$), consistent with experiment. Furthermore, perhaps Zr + C_3H_6 is more efficient because a larger fraction of collisions is able to make the requisite nonradiative transition, driven by the larger density of rovibronic states. In this mechanism, the B3LYP calculations that find no energy barrier to association on the lowest adiabatic potential surface would be correct.

For the present, the simplest picture of Zr + ethylene invokes the existence of a small potential barrier to complex formation on the adiabatic ground state. Within the limits of our approximate statistical rate model, the calculations indicate that the barrier height need be only 0.5−2 kcal/mol. The B3LYP result for TS_{ins} must then be lowered by 3−6 kcal/mol, consistent with the performance of B3LYP on other similar chemical reaction barriers.[1−3] Our preliminary single-point calculation at the B3LYP/Stuttgart+6-311++G(d,p) level of theory with the approach distance fixed at $R = 3.5$ Å indeed suggests a small barrier. More extensive calculations remain highly desirable.

VI. Conclusion

The combination of theory and experiment has led to a remarkably detailed view of the Zr + alkene reaction. The absence of kinetic isotope effects rules out the possibility of direct CH bond insertion of C_2H_4 and C_3H_6 by Zr at low collision energy. Ab initio studies confirm that formation of a metallacyclopropane complex precedes CH bond insertion and subsequent elimination of H_2, although statistical rate modeling adjusts the computed B3LYP/LANL2DZ energies along the reaction path for Zr + ethylene. The combination of higher levels of theory (i.e., multireference CI calculations) with more realistic basis sets may reveal the association barrier implicated in this paper and by the earlier work of Willis et al.[10] Our preliminary results with the larger Stuttgart basis set suggest that B3LYP may well find a small barrier in the limit of large basis set. It would be most satisfying to determine the magnitude of the barrier *experimentally*. Toward that goal, we plan to pursue experimental studies of Zr + alkene in a crossed-beam apparatus at collision energies as low as 0.5 kcal/mol. Similar flow tube studies of ground state Y and Nb with ethylene and propylene, now in progress, should lead to a consistent and more comprehensive mechanistic picture of the M + alkene reaction.

Acknowledgment. We thank the National Science Foundation (CHE-9616724) and the donors of the Petroleum Research Foundation (PRF-33441-AC6) for generous support of this research.

References and Notes

(1) Yi, S. S.; Blomberg, M. R. A.; Siegbahn, P. E. M.; Weisshaar, J. C. *J. Phys. Chem.* **1998**, *102*, 395.

(2) Blomberg, M. R. A.; Siegbahn, P. E. M.; Yi, S. S.; Noll, R. J.; Weisshaar, J. C. *J. Phys. Chem. A* **1999**, *103*, 7254.

(3) Yi, S. S.; Weisshaar, J. C.; Holthausen, M. C.; Koch, W. Work in progress.

(4) Ritter, D.; Carroll, J. J.; Weisshaar, J. C. *J. Phys. Chem.* **1992**, *96*, 10636.

(5) Carroll, J. J.; Haug, K. L.; Weisshaar, J. C. *J. Am. Chem. Soc.* **1993**, *115*, 6962.

(6) Carroll, J. J.; Haug, K. L.; Weisshaar, J. C.; Blomberg, M. R. A.; Siegbahn, P. E. M.; Svensson, M. *J. Phys. Chem.* **1995**, *99*, 13955.

(7) Carroll, J. J.; Weisshaar, J. C.; Siegbahn, P. E. M.; Wittborn, C. A. M.; Blomberg, M. R. A. *J. Phys. Chem.* **1995**, *99*, 14388.

(8) Carroll, J. J.; Weisshaar, J. C. *J. Phys. Chem.* **1996**, *100*, 12355.

(9) Wen, Y.; Porembski, M.; Ferrett, T. A.; Weisshaar, J. C. *J. Phys. Chem. A* **1998**, *102*, 8362.

(10) Willis, P. A.; Stauffer, H. U.; Hinrichs, R. Z.; Davis, F. H. *J. Phys. Chem. A* **1999**, *103*, 3706.

(11) Porembski, M.; Weisshaar, J. C. Work in progress.

(12) Blomberg, M. R. A.; Siegbahn, P. E. M.; Svensson, M. *J. Phys. Chem.* **1992**, *96*, 9794.

(13) Siegbahn, P. E. M.; Blomberg, M. R. A.; Svensson, M. *J. Am. Chem. Soc.* **1993**, *115*, 1952.

(14) Siegbahn, P. E. M. *Theor. Chim. Acta* **1994**, *87*, 277.

(15) Frisch, M. J.; Trucks, G. W.; Schlegel, H. B.; Scuseria, G. E.; Robb, M. A.; Cheeseman, J. R.; Zakrzewski, V. G.; Montgomery, J. A.; Stratmann, R. E.; Burant, J. C.; Dapprich, S.; Millam, J. M.; Daniels, A. D.; Kudin, K. N.; Strain, M. C.; Farkas, O.; Tomasi, J.; Barone, V.; Cossi, M.; Cammi, R.; Mennucci, B.; Pomelli, C.; Adamo, C.; Clifford, S.; Ochterski, J.; Petersson, G. A.; Ayala, P. Y.; Cui, Q.; Morokuma, K.; Malick, D. K.; Rabuck, A. D.; Raghavachari, K.; Foresman, J. B.; Cioslowski, J.; Ortiz, J. V.; Stefanov, B. B.; Liu, G.; Liashenko, A.; Piskorz, P.; Komaromi, I.; Gomperts, R.; Martin, R. L.; Fox, D. J.; Keith, T.; Al-Laham, M. A.; Peng, C. Y.; Nanayakkara, A.; Gonzalez, C.; Challacombe, M.; Gill, P. M. W.; Johnson, B.; Chen, W.; Wong, M. W.; Andres, J. L.; Head-Gordon, M.; Replogle, E. S.; Pople, J. A. *Gaussian 98*, revision A.6; Gaussian, Inc.: Pittsburgh, PA, 1998.

(16) Moore, C. E. *NBS Circ. No. 467*; U. S. Department of Commerce: Washington, DC, 1949; Vols. I−III.

(17) Andrae, D.; Häussermann, U.; Dolg, M.; Stoll, H.; Preuss, H. *Theor. Chim. Acta* **1990**, *77*, 123.

(18) Robinson, P. J.; Holbrook, K. A. *Unimolecular Reactions*; Wiley-Interscience: New York, 1972.

(19) Gilbert, R. G.; Smith, S. C. *Theory of Unimolecular and Recombination Reactions*; Blackwell Scientific Publications: Oxford, U.K., 1990.

(20) Baer, T.; Hase, W. L. *Unimolecular Reaction Dynamics*; Oxford University Press: New York, 1996.

(21) Carroll, J. J. Thesis, Univeristy of Wisconsin-Madison, 1995.